THE JOURNAL OF PHYSICAL CHEMISTRY B

Article

pubs.acs.org/JPCB

Comparative Studies on IR, Raman, and Surface Enhanced Raman Scattering Spectroscopy of Dipeptides Containing ΔAla and ΔPhe

Kamilla Malek,*[,†] Maciej Makowski,[‡] Agata Królikowska,[§] and Jolanta Bukowska[§]

[†]Faculty of Chemistry, Jagiellonian Chemistry, Ingardena 3, 30-060 Krakow, Poland

[‡]Institute of Chemistry, University of Opole, Oleska 48, 45-052 Opole, Poland

[§]Faculty of Chemistry, University of Warsaw, Pasteura 1, 02-093 Warsaw, Poland

Supporting Information

ABSTRACT: Three dipeptides containing dehydroresidues (ΔAla, $\Delta^{(Z)}$Phe, and $\Delta^{(E)}$Phe) were examined by IR, Raman, and surface-enhanced Raman techniques for the first time. The effect of the size and isomer type of the β-substituent in the dehydroresidue on the conformational structure of the peptide was evaluated by using the analysis of IR and Raman bands. Additionally, SERS spectroscopy provided insight into the adsorption mechanism of these species on the metal surface. SERS spectra were recorded at alkaline pH on the silver sol using visible light excitation. The dehydroresidues studied here strongly influenced the SERS profile of the peptides. The most pronounced SERS signal for all dipeptides was assigned to the symmetric stretching vibration of the carboxylate ions. This indicates that the dehydropeptides studied here primarily adsorb via the deprotonated carboxylic group. Additionally, the enhanced SERS bands in the range 1550−1650 cm^{-1} show differences in contribution of the dehydroresidue to the adsorption mechanism of the studied peptides.

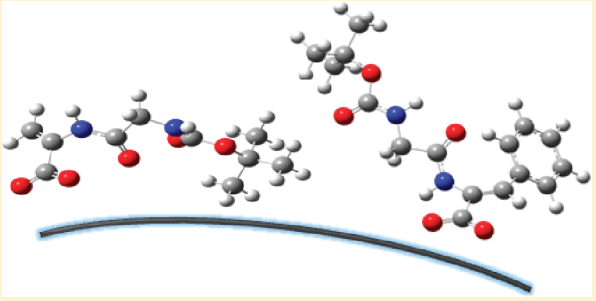

1. INTRODUCTION

Among the family of natural peptides, some amino acids (dehydroamino acids) are modified into the unsaturated form, in which the double C_α=C_β bond is present. This change of a tetrahedral structure around C_α into a trigonal arrangement induces specific steric effects, which influence the secondary structure of dehydropeptides. This modified unit has been found in a number of naturally occurring peptides, like nisins,[1] thiopeptide antibiotics,[2] or microcystins,[3] and is related to biocatalysis.[4−6] The incorporation of the dehydroamino acids into peptide hormones, e.g., enkephalin, bradykinin, or thyrotropin-releasing hormone, has resulted in changing the hormone agonist or antagonist activity.[7] The recent studies have shown that this class of peptides exhibits also unusual binding properties toward transition metal ions in comparison to their saturated analogues.[8] Dehydroalanine (ΔAla) and dehydrophenylalanine (ΔPhe) are the most known natural dehydroamino acids. In the case of the latter, the two isomers can be distinguished, namely *Z* (*zusammen* = together) and *E* (*entgegen* = opposite). $\Delta^{(Z)}$Phe is energetically preferred and more common in nature. The conformational preferences of the dehydropeptides strongly depend on the flatness of a dehydroamino acid and the size and shape of its side substituents. A more pronounced effect of the steric constraints on the geometry has been found for ΔAla than for ΔPhe. Hence, the ΔAla peptides adopt usually a flat *trans* extended configuration, while the presence of ΔPhe in peptides generates folded as well as extended conformations.[9] Furthermore, dehydropeptides usually form stronger H-bonding than their saturated counterparts.[9,10] Conformational studies on a series of dipeptides with the ΔAla residues and their saturated counterparts have shown that the presence of this dehydroresidue encourages the formation of a γ-turn, which in order cannot be stabilized by the flexible Ala.[7,9] In the case of a folded conformation, the peptide sequence introducing (*Z*)-dehydrophenylalanine often tends to permit both left-handed and right-handed helices, mostly of the 3_{10}-helical and β-turn and sometimes of the α-helical type.[9,11] On the other hand, the $\Delta^{(E)}$Phe residue is a part of a type II β-turn in the crystalline state of penta- and hexapeptides.[12−14] Long peptides with more than one ΔPhe unit favor usually 3_{10}-helical structures. However, a novel β-bend ribbon conformation has been observed in many pentapeptides containing two ΔPhe residues, while occurrence of next/more than two ΔPhe residues in peptides stabilizes a left-handed helical conformation (see ref 15 and references therein). Similarly, quantum mechanical studies have demonstrated that the poly(ΔAla) sequence is a better helical former than Ala.[16] Thus, this class of peptides has often been designed for their potential use as protein mimics and as an effective tool in modeling of the precise secondary structures of peptides and proteins. The conformational preferences of dehydropeptides are related to the contribution of the resonance between C=O and the C=C/styryl groups within a dehydroresidue, especially for ΔPhe due to extended

Received: September 6, 2011
Revised: November 23, 2011
Published: December 30, 2011

conjugation of the ring electrons and the remaining part of the residue. It was shown experimentally that the C_α—$C_{C=O}$ bond length of dehydroresidues is slightly shorter than the corresponding length of the saturated residues. This resonance affects also bond lengths of the peptide bond and a side-chain group and consequently leads to steric contacts between the side-chain and main-chain atoms. As expected, this unfavorable steric hindrance is minimized by a spatial rearrangement of bond angles around a dehydroresidue.[9,15,17] Up to now, vibrational studies on this class of peptides have been limited to conformational studies with use of IR spectroscopy, supported by quantum chemical calculations.[10,11,17−19] To our best knowledge, there is no information in the literature about its Raman spectra and on the adsorption on the metal surface investigated with surface-enhanced Raman spectroscopy (SERS).

The present work reports the first part of a series of our investigations devoted to the analysis of vibrational properties of dehydropeptides, including their adsorption on silver colloidal particles. Here, our attention is basically focused on three didehydropeptides containing ΔAla (Boc-Gly-ΔAla), $\Delta^{(Z)}$Phe (Boc-Gly-$\Delta^{(Z)}$Phe), and Δ(E)Phe (Boc-Gly-$\Delta^{(E)}$Phe); see Scheme 1. The *tert*-butyloxycarbonyl group (Boc) was introduced to the structure of the peptides to block the N-terminal end of the peptide. Its role is to mimic a polypeptide chain attached to this end of the molecule, and it enables investigation of the effect of the dehydroresidue at the C-terminal on a conformation in the solid state and adsorption mechanism on the silver surface. From the experimental point of view, we present newly recorded normal Raman spectra (NR) of the peptides complemented by their FT-IR spectra of the samples in the solid state and solution. Further insight into the molecular structure and the theoretical modeling of the vibrational profile are provided by DFT (density functional theory) calculations. The unambiguous assignment of the observed IR and Raman bands is performed by using potential energy distribution (PED) calculations. These calculations are performed also in order to evaluate the substituent effect on the conformational structure of the chosen didehydropeptides. Next, we examine the nature of interactions of the selected dehydropeptides with the silver surface utilizing surface plasmon enhancement, and also determine how the presence of chemically and spatially different dehydroresidues affects the peptides' ability of adsorption on the colloidal Ag particles. It should be stressed here that SERS spectroscopy has become an important method for the characterization of biomolecules and monitoring processes in which they are involved.[20−22] Very large enhancements of the effective Raman signal make this technique useful for the sensitive and selective detection of submolar concentration analytes, providing information regarding metal−adsorbate interactions.[23,24] Another advantage of SERS is an effective quenching of fluorescence background, which is commonly strong in the normal Raman spectra of bioanalytes. Thus, these studies can contribute to a future understanding of the SERS profile of complex biospecies containing a dehydroresidue by providing the SERS characteristics of their short subunits. Additionally, it may support the understanding of the nature of the high affinity of the dehydropeptides to transition metals.[8] Moreover, to our best knowledge, no simultaneous IR, Raman, and SERS analysis of the peptides containing dehydroamino acid has been reported in the literature up to now. This manuscript may be considered as the first report of the full vibrational assignment of dehydropeptides, providing additionally initial elucidation of the adsorptive behavior.

Scheme 1. Molecular Structures of the Dehydropeptides Studied[a]

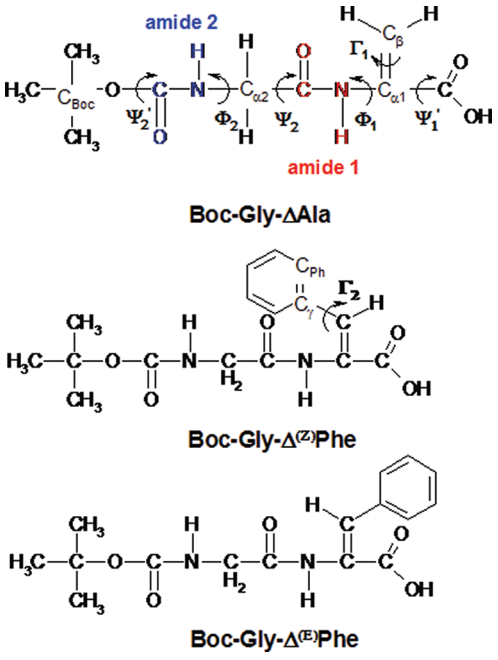

[a]Greek symbols with arrows refer to the torsion angles collected in Table 1 and discussed in the text.

2. EXPERIMENTAL METHODS

2.1. Preparation of Samples. Dehydropeptides were synthesized according to the procedure in refs 25−27. Briefly, dipeptides were synthesized in a condensation reaction between the trifluoroacetate (TFA) amide of alanine or phenylalanine and α-keto acid (pyruvic acid or phenylpyruvic acid) in benzene. The reaction is catalyzed by *p*-toluenesulfonic acid. In the case of TFA-Gly-ΔPhe, both isomers (*Z* and *E*) are formed in a ratio of 4:1. Then, the TFA group is substituted by the Boc group. Yield: ca. 50% for all compounds.

The solid samples were dissolved in methanol (concentration of 1 M) because of the very low solubility of the studied dehydropeptides in water. The final concentrations of 0.1 and 1 × 10^{-3} M were prepared by dilution of the stock solution with water. The pH of the analyte solutions (11) was adjusted by adding 0.01 M NaOH. All employed reagents were of analytical grade and purchased from Sigma-Aldrich. Aqueous solutions were prepared by using 4-fold distilled water.

2.2. SERS Experiment. Silver colloid was prepared following Creighton's procedure,[28] by adding silver nitrate to an aqueous solution of excess sodium borohydride as a reducing agent. The UV−vis spectra of colloids were recorded in a quartz cell of 1 cm path length, with an Evolution 60 spectrophotometer in the region 190−1100 nm, achieving a spectral resolution of 1 nm. Two batches of colloids were prepared, and their resonant absorption bands appeared in the range 390−396 nm. The position of the absorption maximum indicates that the size of silver nanoparticles varies in the range 10−50 nm.[28,29] To prepare a sample for SERS measurements, 20 μL of 1 mM dehydropeptide samples at a pH of 6 and 11

dx.doi.org/10.1021/jp208586j | J. Phys. Chem. B 2012, 116, 1414−1425

was added to 1 mL of the colloid, activated with 40 μL of 0.5 M KCl or KNO_3. The activation of the colloid results in a homogeneous aggregation of Ag nanoparticles that in turn gives the greatest surface enhancements and more reliable SERS spectra.[30] The final concentration of the dehydropeptide in the sample was 0.01 mM. We did not change the pH of the colloid above 9 to avoid changes in morphology of the silver colloids.

2.3. Instrumentation. Fourier transform mid-infrared (FT-MIR, 256 scans) spectra of the solid samples were run in KBr pellets with a resolution of 4 cm^{-1}. FT-IR spectra were measured with a Bruker (IFS 48) spectrometer in the region 400−4000 cm^{-1}. Frequency accuracy is estimated to ±1 cm^{-1}.

For FT-Raman measurements (NR), a few milligrams of solid dehydropeptides and their 0.1 M solutions at a pH of 6 and 11 were directly measured on metal discs and glass cuvettes, respectively. 512 and 4000 scans were collected (with a resolution of 4 cm^{-1}) for solid and solution samples, respectively. Spectra were recorded with the FT-Raman Spectrometer Bruker Ramanscope III equipped with a Nd:YAG laser, emitting at 1064 nm, and a germanium detector cooled with liquid nitrogen. The output power of the laser was 50 and 300 mW for solid and solution samples, respectively.

SERS spectra of adsorbates and Raman spectra of solid samples were collected in the backscattering configuration with a Labram HR800 (Horiba Jobin Yvon) confocal microscope system, equipped with a Peltier-cooled CCD detector (1024 × 256 pixels), using a diode pumped, frequency doubled Nd:YAG laser (532 nm). The output laser power (on the head) was 100 mW. The confocal pinhole size was set to 200 μm, and the holographic grating with 600 grooves/mm was used. The calibration of the instrument was performed using the 520 cm^{-1} Raman signal of a silicon wafer. SERS spectra were collected twice in two different batches of the Ag colloid. For colloidal solution measurements, a cuvette holder and 1 cm quartz cuvette were used. For each SERS spectrum, four scans were collected with an integration time of 10 s. Raman spectra of the solid samples were obtained using a 50× magnification Olympus objective and accumulating 1−5 scans, ranging from 3 to 20 s.

2.4. Computational Details. Density functional theory (DFT) calculations were carried out for geometry optimization and simulation of vibrational spectra. These calculations were performed with the Gaussian 09 program package.[31] First potential energy surfaces were investigated in order to localize the stable conformers with respect to the Φ_1 dihedral angle (see Scheme 1) around the unsaturated moiety by using the B3LYP method[32,33] and the 6-31+G(d) basis set. Next, the structures in the energetic minima were chosen to perform full optimization at the B3LYP/6-311++G(d,p) level of theory. No imaginary frequencies were obtained. Calculations were carried out for protonated forms of the studied molecules *in vacuo*. We would like to emphasize that these calculations were aimed to obtain the structural variation caused by the presence of the various dehydroresidues rather than the absolute minima, which would have no meaning in the present context because the peptide structure is known to be a state of matter and solvent dependent. Next, theoretical Raman intensities (I^R) were obtained from Gaussian Raman scattering activities (S) according to the expression[34] $I_i^R = 10^{-12}(\nu_0 - \nu_i)^4\nu_i^{-1}S_i$, where ν_0 is the excitation frequency (9398.5 cm^{-1} for Nd:YAG laser) and ν_i is the frequency of the normal mode calculated by DFT. Prior to comparing the calculated wavenumbers with their experimental counterparts, we used the appropriate scaling factors, i.e., 0.98 and 0.96 for the 0−2000 and 2001−4000 cm^{-1} regions, respectively. To provide the unequivocal assignment of the calculated IR and Raman spectra, the potential energy distribution (PED) analysis was performed by using the Gar2ped software.[35−37] The program first defines a set of nonredundant internal coordinates according to the Pullay and Foragasi definitions, and next, the percentage contribution of these internal coordinates to the total energy of each normal mode is computed. Definitions of the internal coordinates used in this work are collected in Table S1 in the Supporting Information.

3. RESULTS AND DISCUSSION

3.1. Molecular Structure. To find a preferable configuration around the dehydroresidue, we computed potential energy values for a series of values of the Φ_1 dihedral angle (see Scheme 1). The model molecules are the protonated form of the dipeptides. Then, the full optimization process was performed for structures found in minima of potential energy for a given Φ_1. In this way, we evaluated the effect of each dehydroresidue on the conformation of the dipeptides. The calculated molecular structures in energetic minima are shown in Figure 1. In turn, Table 1 lists the computed angles Φ, Ψ (typical in determination of the conformational structure of the peptides), and Γ (around the unsaturated moieties). The labeling of the angles is depicted in Scheme 1. To the best of our knowledge, no X-ray crystallographic data of the presented

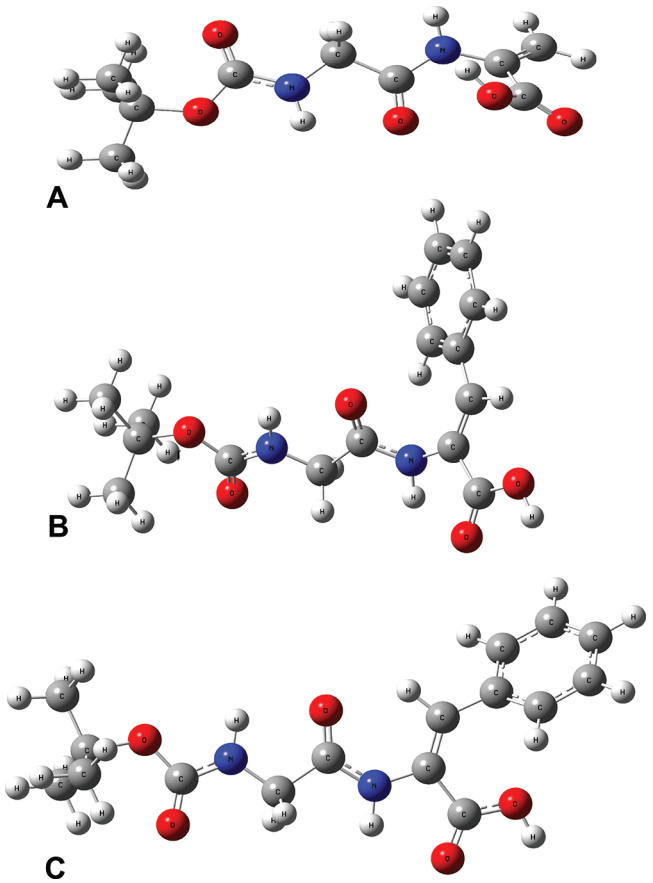

Figure 1. The optimized structures of Boc-Gly-ΔAla (A), Boc-Gly-$\Delta^{(Z)}$Phe (B), and Boc-Gly-$\Delta^{(E)}$Phe (C) by using B3LYP/6-311++G(d,p).

dx.doi.org/10.1021/jp208586j | J. Phys. Chem. B 2012, 116, 1414−1425

Table 1. Selected Dihedral Angles (in Degrees) of the Dehydropeptides from DFT Optimized Structures[a]

torsion angles	Boc-Gly-ΔAla	Boc-Gly-$\Delta^{(Z)}$Phe	Boc-Gly-$\Delta^{(E)}$Phe
$\Psi_1'(O_C C_C C_{\alpha 1} N)$	156.1	−177.3	−170.0
$\Phi_1(C_C C_{\alpha 1} NC)$	151.5	127.1	179.2
$\Psi_2(NCC_{\alpha 2} N)$	174.7	179.6	173.6
$\Phi_2(CC_{\alpha 2} NC)$	−169.3	−168.6	−173.6
$\Psi_2'(NCOC_{Boc})$	−179.9	−178.9	−179.2
$\Gamma_1(HNC_{\alpha 1} C_\beta)$	137.7	156.5	179.9
$\Gamma_2(C_{\alpha 1} C_\beta C_\gamma C_{Ph})$		165.9	139.5

[a]Scheme 1 depicts labeling of the angles.

molecules has yet been established. However, as discussed in the Introduction, structural studies on other dehydropeptides have revealed that insertion of the double bond in the alanine residue usually leads to the fully extended conformations with Ψ, $\Phi \approx -180°$, 180°.[9,38] While the introduction of ΔPhe results in folded conformations, e.g., β-turn and helices.[13,39] The calculated Φ_1, Ψ_1' angles differ significantly for the dipeptides studied here. The Φ_1/Ψ_1' angles of Boc-Gly-$\Delta^{(Z)}$Phe (127.1/−177.3°) are typical for the single dehydroresidue structures with different blocking groups,[9,10,19,40] suggesting a preference of these dipeptides to form an extended C_5 conformation. Interestingly, the change of the isomer type from *Z* to *E* leads to a fully extended conformation, since the Φ_1/Ψ_1' angles are close to 180°, on the contrary to a β-turn conformation found for long peptides containing $\Delta^{(E)}$Phe.[12−14] The extended structure ensures the most effective π-electron cross-conjugation. Similarly to Boc-Gly-$\Delta^{(Z)}$Phe, the Gly-ΔAla fragment adopts the extended C_5 conformation, with Φ_1/Ψ_1' angles of around 151.5/156.0° what is found in the agreement the conformational preference of this dehydroresidue.[9,40] Here, the larger deviation from planarity of the torsion angle Ψ_1' than that in the ΔPhe peptides results from a stability of the Boc-Gly-ΔAla structure by an internal H-bond and the C_β—H···O=C^{COOH} cross-conjugation (H···O distance: 2.47 Å).[40] The latter is excluded for the ΔPhe derivatives (cf. Figure 1). The examination of the optimized molecular structures of the studied dipeptides can suggest that the observed conformations are stabilized by intramolecular C=O^{amideI}···H^{COOH} and N—H^{amideI}···O=C^{COOH} hydrogen bonds for Boc-Gly-ΔAla and Boc-Gly-ΔPhe, respectively (see Figure 1). The calculated H···A distances are 1.65, 2.23, and 2.07 Å in structures of the ΔAla, $\Delta^{(Z)}$Phe, and $\Delta^{(E)}$Phe derivatives, respectively. The different H-bonding is undoubtedly the reason for the various spatial arrangements of the carboxylic group with respect to the peptide backbone. Next, the remaining fragment of the molecules (Boc-Gly) is not strongly affected by the unsaturated residues, as the computed values of the Ψ_2, Φ_2, and Ψ_2' angles reveal. The Ψ and Φ angles for the glycine residue are characteristic for an extended conformation. Additionally, the dihedral angle $HNC_\beta C_{\alpha 1}$ (Γ_1) determines an orbital overlap between the π-systems of the amide and the $C_{\alpha 1}$=C_β bonds in the dipeptides. Boc-Gly-$\Delta^{(E)}$Phe shows coplanarity of both groups (Γ_1: 180°), whereas the π-electron resonance is reduced for $\Delta^{(Z)}$Phe (Γ_1: 156°) and ΔAla (Γ_1: 138°). As expected, the *Z* and *E* isomers of ΔPhe strongly affect the spatial arrangement of the phenyl ring that is rotated with respect to the peptide backbone by 14 and 40° (Γ_2), respectively. Thus, a π-conjugation between the phenyl ring of $\Delta^{(Z)}$Phe and $C_{\alpha 1}$=C_β likely occurs, whereas the tilted orientation of the phenyl ring in the *E* isomer can weaken this electron redistribution. Additionally, the *Z* conformer is calculated to have 8.3 kJ·mol^{-1} lower energy (according to zero-point-corrected energies) than the *E* form, which is in agreement with the common abundance of the $\Delta^{(Z)}$Phe peptides in nature.

3.2. Normal Raman and IR Spectra of the Molecules and Band Assignment. Figures 2 and 3 depict, respectively,

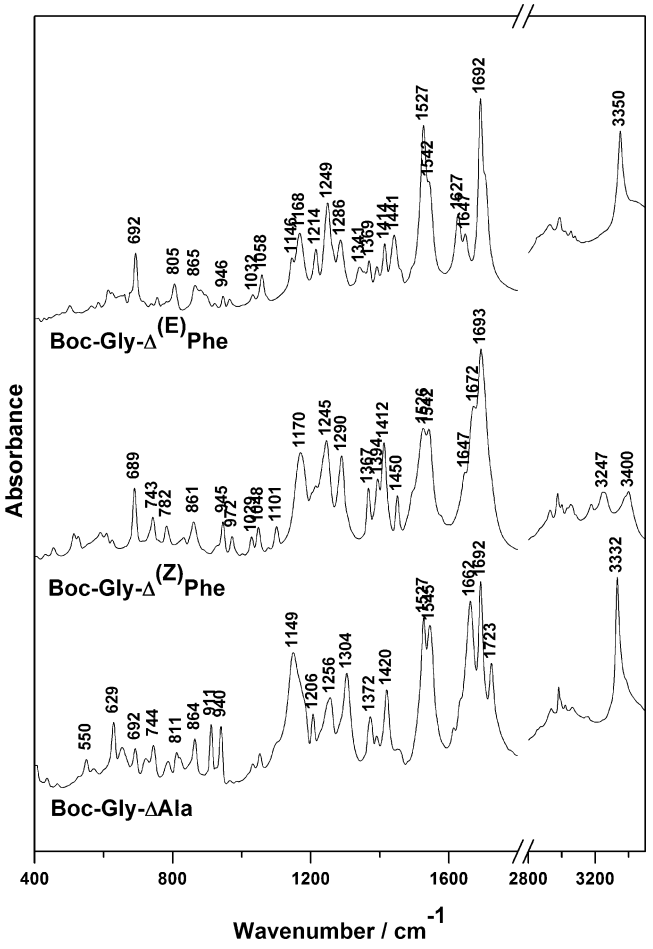

Figure 2. FT-IR spectra of the dehydropeptides of neat powder in a KBr pellet in the spectral range 400−3500 cm^{-1}.

IR and normal Raman spectra of the solid state of the dehydropeptides. Assignments of the selected bands based on calculations of potential energy distribution (PED) are collected in Tables 2−4. Definitions of internal coordinates are listed in Table S1, while the comparison of the theoretical and experimental spectra is shown in Figures 1S−3S (Supporting Information). Below, we provide a brief discussion on the most pronounced IR and Raman bands that can reveal spectral information on the structure. This assignment is used in the further discussion on the metal−adsorbate interactions.

The position of ν(NH) (amide A mode) provides some information on the type of conformation due to N−H···O interaction. IR and Raman bands observed over 3400 cm^{-1} originate from free NH groups, whereas bands between 3100 and 3400 cm^{-1} have often been attributed to folding of a secondary structure or to intra- and intermolecular H-bonding as observed for other dehydropeptides.[7,11,17,19] As shown in the previous section, the intramolecular H bonding between the carboxylic group and the neighboring amide bond is possible. However, intermolecular H-bonding is also observed in the

dx.doi.org/10.1021/jp208586j | J. Phys. Chem. B 2012, 116, 1414−1425

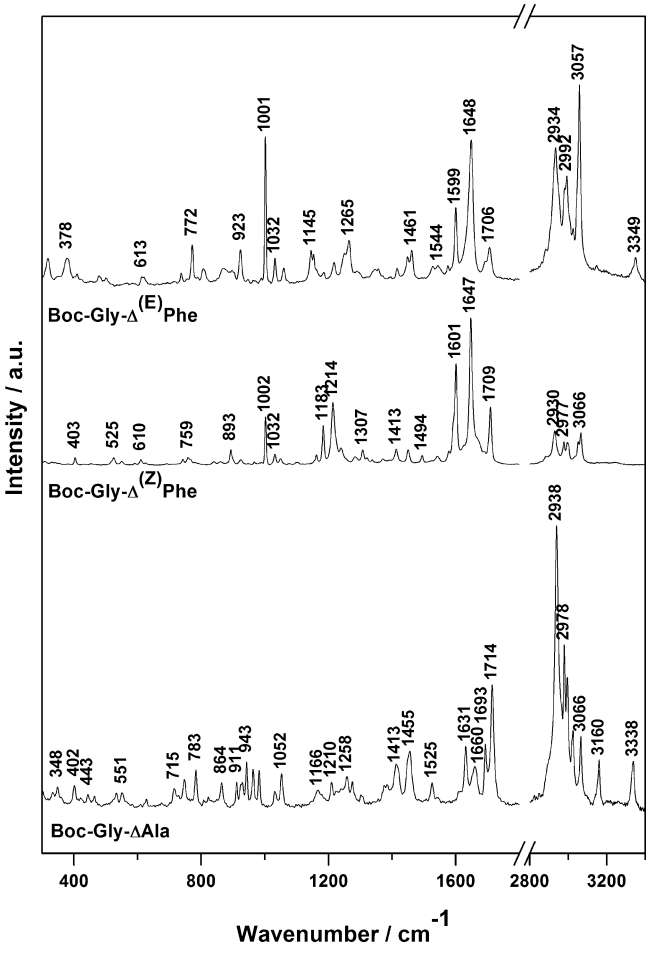

Figure 3. FT-Raman spectra of the solid dehydropeptides in the spectral range 300−3400 cm^{-1} (an excitation line at 1064 nm).

solid state of dehydropeptides.[12−14] Amide A vibrations are observed in the IR spectra at 3332 (vs), 3400/3247 (m), and 3350 (vs) cm^{-1} for Boc-Gly-ΔAla, Boc-Gly-$\Delta^{(Z)}$Phe, and Boc-Gly-$\Delta^{(E)}$Phe, respectively (Figure 2). The strong and narrow IR absorption in the NH stretching region for Boc-Gly-ΔAla and Boc-Gly-$\Delta^{(E)}$Phe indicates that these compounds exist in one conformation, probably in the open or extended form with an internal hydrogen bond. The lower wavenumber of ν(NH) for the peptide with ΔAla suggests stronger H-bonds in that case than for $\Delta^{(E)}$Phe. Inflections on the high wavenumber edge of both bands suggest that the presence of free N−H groups is marginal. On the other hand, the appearance of a weak amide A band at 3247 cm^{-1} in the IR spectrum of Boc-Gly-$\Delta^{(Z)}$Phe can indicate association of the molecules through the N−H groups.[41] In turn, the next amide A band observed at 3400 cm^{-1} may indicate free or weakly affected by intermolecular interactions NH bonds.

The amide 1 vibrations can be affected by H-bonding and/or π-electron conjugation with the C═C bond.[11] The IR and Raman spectra of the studied peptides exhibit the presence of a few bands in the region 1580−1730 cm^{-1} (cf. Figures 2 and 3). Our DFT calculations revealed that the strongest IR band in this region should be assigned to the amide I vibration (%PED: 87, 72, and 44 for Boc-Gly-ΔAla, Boc-Gly-$\Delta^{(Z)}$Phe, and Boc-Gly-$\Delta^{(E)}$Phe, respectively) of the group adjacent to the Boc moiety ("amide 2" in Scheme 1, Tables 2−4). Thus, this mode is attributed to a band at 1692 cm^{-1} in IR spectra (Figure 2). This high wavenumber hints at the shortness of the C═O bond length (calc.: 1.22 Å in all peptides). Likely, this amide group is involved strongly in neither intra- nor intermolecular H-bonds, as it is protected by the Boc group. The amide I mode (amide I_1) of the group adjacent to the unsaturated moiety ("amide 1" in Scheme 1) is observed at 1662 and 1672 cm^{-1} in IR (cf. Figure 2) for Boc-Gly-ΔAla and Boc-Gly-$\Delta^{(Z)}$Phe, respectively, whereas the IR spectrum of Boc-Gly-$\Delta^{(E)}$Phe shows the presence of two medium-intensity IR bands at 1627 and 1648 cm^{-1}. One could assign a band at 1648 cm^{-1} in IR to the amide I_1 vibration. However, an analysis of the Raman spectra supported by DFT calculations indicates that this band should be attributed to the ν(C═C) mode. Figure 4 shows the comparison of experimental and theoretical Raman spectra in the region 1550−1750 cm^{-1}. On the basis of the appearance order in the simulated spectra, the experimental bands over 1700 cm^{-1} are assigned to the ν(C═O) mode of the carboxylic group for all peptides, while ν(C═C) appears at 1631 and 1647 cm^{-1} for Boc-Gly-ΔAla and (*Z* and *E*) Boc-Gly-ΔPhe, respectively. Therefore, we assigned the amide I_1 band of Boc-Gly-$\Delta^{(E)}$Phe to a medium IR band at 1627 cm^{-1}. Summarizing, wavenumbers of amide I_1 appear in IR at 1627, 1662, and 1672 cm^{-1} for Boc-Gly-$\Delta^{(E)}$Phe, Boc-Gly-ΔAla, and Boc-Gly-$\Delta^{(Z)}$Phe, respectively. IR studies on long dehydropeptides have reported[11,18] that amide I absorption bands centered at ca. 1650−1670 and 1630 cm^{-1} are usually diagnostic of monomeric α helical and β-sheet structures, respectively. On the other hand, IR spectra of a series of *N*-acetyl-dehydroamino acid *N*′-methyl amides (with ΔAla, $\Delta^{(Z)}$Abu, ΔLeu, ΔVal, $\Delta^{(Z)}$Phe) show the appearance of amide I bands in the region 1663−1698 cm^{-1}.[19] All of them adopt a fully extended C_5 conformation. On the basis of these results, the determination of a conformation for Boc-Gly-ΔAla and Boc-Gly-$\Delta^{(Z)}$Phe from their IR spectra is not equivocal. Thus, the positions of the amide I bands of peptides studied here must reflect the differences in the strength of hydrogen bonding as well as electron density perturbation induced by dehydroresidue.[11,17,19] We attempted to address the question of electronic interaction between C═O and C═C bonds by using our DFT results performed *in vacuo*. The greater amide distortion from planarity is observed for Boc-Gly-ΔAla and Boc-Gly-$\Delta^{(Z)}$Phe than for Boc-Gly-$\Delta^{(E)}$Phe (Φ_1 in Table 1). Next the computed C═O bond lengths of the amide 1 bond are similar (ca. 1.21 Å) for the ΔAla and $\Delta^{(Z)}$Phe derivatives but shorter than for the $\Delta^{(E)}$Phe residue (1.23 Å). This is consistent with the higher wavenumber of amide I_1 for the ΔAla and $\Delta^{(Z)}$Phe peptides in the experimental IR spectra. On the other hand, the lengths of the C═C bonds are ca. 1.35 and 1.33 Å for Boc-Gly-ΔAla and Boc-Gly-ΔPhe; therefore, ν(C═C) is down-shifted in the Raman spectrum Boc-Gly-ΔAla in comparison with Boc-Gly-ΔPhe, as shown above. Hence, some resonance structures of the dehydroamides can be deduced as Scheme 2 shows.[10] We propose that resonance structures II, I, and III participate to a larger extent in Boc-Gly-ΔAla, Boc-Gly-$\Delta^{(Z)}$Phe, and Boc-Gly-$\Delta^{(E)}$Phe, respectively. The lengthening of the C═C bond in ΔAla results probably from a shift of the $\pi_{C=C}$ electrons toward the amide C atom; however, non-planarity of the H_2C═C—CO—NH moiety (Γ_1 in Table 1) prevents mutual resonance within this group. Therefore, the C═O bond may conserve its "double" character. Next, the similar nature of the C═O bond is observed in $\Delta^{(Z)}$Phe; however, the shortening of the C═C bond occurs. This may be explained by the π-electron-donating effect from the attached phenyl ring, since the C═C and the

dx.doi.org/10.1021/jp208586j | J. Phys. Chem. B 2012, 116, 1414−1425

Table 2. Positions of the Selected IR, Raman, and SERS Bands (in cm^{-1}) of Boc-Gly-ΔAla and Their Assignments (in %, PED >10% Shown) Based on Calculations[a]

FT-IR[b]	FT-NR[b]	SERS	assignment
3332vs	3338m		100 ν(NH)
	3160m		99 $\nu_{as}(=CH_2)$
	3066m		99 $\nu_{s}(=CH_2)$
	3024m		95 $\nu_{as}(CH_3)_{Boc}$
	2994m		84 $\nu_{as}(CH_3)_{Boc}$
	2978s		96 $\nu_{as}(CH_3)_{Boc}$
	2938vs		91$\nu_{s}(CH_3)_{Boc}$
1723m	1714s		76 $\nu(C{=}O)_{COOH}$
1692vs	1693m		87 amide I_2
1662vs	1660m	1651vs	72 amide I_1
1633w,sh	1631m/1641w[c]	1621vs	59 $\nu(C_{\alpha 1}{=}C_{\beta})$
1545vs			58 amide II_1, 21 amide II_2
1527vs	1525w	1511m	58 amide II_2, 24 amide II_1
	1455m	1465/1446m	84 $\delta(CH_3)_{Boc}$
1420m	1413m		80 $\delta(=CH_2)$
1372m	1375vw		44 $\omega(CH_2)_{Gly}$, 10 $\nu(C_{Gly}C)$
		1362vs	$\nu_{s}(COO^{-})$
1304s	1304w	1312w	35 $\nu(CN)_{amide1}$, 18 ν(CC)
	1275w	1289w	41 $\rho(CH_3)_{Boc}$, 29 $\nu(CC)_{Boc}$
1256m	1258w		65 $\tau(CH_2)_{Gly}$
1206m	1210w	1204w	31 amideIII_2, 25 $\omega(CH_2)_{Gly}$
1181s,sh		1181m	37 ν(CN), 28$\nu(C{-}O)_{COOH}$
1149vs			30 $\rho(CH_3)_{Boc}$, 28 $\nu(CO)_{Boc}$
1052w	1052m	1017s	47 $\rho(CH_3)_{Boc}$, 17 $\nu(CO)_{Boc}$
1032vw	1031w		74 $\rho(CH_3)_{Boc}$
	963m		54 $\omega(=CH_2)$
911m	911w	910m	48 $\omega(CH_3)_{Boc}$, 34 $\omega(=CH_2)$
786w	783m	771m	84 $\omega(CO)_{Boc}$
629m	628vw	610s	31 $\beta(COO^{-})$, 25 $\rho(C{=}O)_{amide1}$

[a]B3LYP/6-311++G(d,p). [b]Band positions from the spectra of the solid sample. [c]Raman band positions from the spectra of the solution at pH 11: ν, stretching; δ, scissoring; ρ, rocking; ω, wagging; β, in-plane bending; τ, twisting; s, symmetric; as, asymmetric; vs, very strong; s, strong; m, medium; w, weak; vw, very weak; sh, shoulder.

ring are almost coplanar (Γ_2 in Table 1). On the other hand, the π-conjugation of the amide, double CC bonds, and the carboxylic group seems well developed in the plane conformation (Ψ_1', Φ_1, Γ_1 in Table 1) but with a weak electron influx from the phenyl ring (Γ_2 in Table 1). Therefore, the planarity of this fragment of the peptide backbone may cause an electron flux from the C═O bond leading to its elongation.

The IR spectra of all peptides show strong, well resolved bands with absorbance maxima at ca. 1527 and 1542 cm^{-1} that are assigned to the amide II vibration (Figure 2). It can be seen that this mode is insensitive to the dehydroresidue chemical nature and is found in a region typical for other dehydropeptides.[10,11,17−19]

Up to now, the vibrational characteristic of dehydropeptides has been focused mainly on an analysis of amide bands in order to interpret their conformational structure.[7,9−11,17−19] Here, we also give an assignment of bands that originate from the dehydroresidues. The high wavenumber region of Raman spectra shows the presence of the stretching mode of the ═CH group. For Boc-Gly-ΔAla, two components of medium intensity are visible at 3160 and 3066 cm^{-1} [$\nu_{as}(=CH_2)$ and $\nu_{s}(=CH_2)$, respectively], whereas the ν(═CH) mode of ΔPhe is overlapped by mode 1 of the phenyl ring [ν(CH)] at 3066 and 3057 cm^{-1} for the *Z* and *E* isomers of ΔPhe, respectively. The deformation vibrations of the $=CH_2$ group of ΔAla appear visibly at 1420 [IR, $\delta(=CH_2)$], 1031 [NR, $\rho(=CH_2)$], 963 [NR, $\omega(=CH_2)$], and 911 cm^{-1} [IR,NR, $\gamma(=CH_2)$]. In the case of both ΔPhe peptides, the bands at ca. 1390 (IR) and ca. 924 (NR) cm^{-1} are attributed to the ρ(═CH) and ω(═CH) modes, respectively. The latter is coupled with mode 17b [ω(═CH)] of the phenyl ring.

In the Raman spectra of the peptides containing ΔPhe (in Figure 3), the major stretching C═C mode of the phenyl ring is centered at 1600 cm^{-1} (mode 8a), accompanied by a minor band at 1578 cm^{-1} (8b). Wavenumbers of both vibrations are consistent with typical positions observed in spectra of other compounds with the monosubstituted phenyl ring.[37] The most pronounced vibration of Ph (the breathing mode, 12) occurs as a sharp and strong band at 1000 cm^{-1} with a shoulder at 1032 cm^{-1} (the in-plane bending mode, 18a). As mentioned above, the stretching mode of the $C_{\alpha 1}{=}C_{\beta}$ bond appears also at the same position for both isomers (1647 cm^{-1} in Raman). However, significant changes of relative integrated intensities of 8a, 12, and ν(C═C) are observed. Namely, we remarked that $I_{C\alpha 1=C\beta}/I_{8a}$ is 1.6 and 4.3, whereas I_{8a}/I_{12} amounts to 4.6 and 0.8 for $\Delta^{(Z)}$Phe and $\Delta^{(E)}$Phe, respectively (see Figure 3). The former observation can be explained by a resonance effect between the phenyl ring and the $C_{\alpha 1}{=}C_{\beta}$ bond. As our computation showed, the values of the Γ_2 angle determining overlapping $\pi_{C\alpha 1=C\beta}$ and π_{Ph} orbitals is smaller for the $\Delta^{(Z)}$Phe derivative than for $\Delta^{(E)}$Phe (Table 1). The greater overlap

dx.doi.org/10.1021/jp208586j | J. Phys. Chem. B 2012, 116, 1414−1425

Table 3. Positions of the Selected IR, Raman, and SERS Bands (in cm^{-1}) of Boc-Gly-$\Delta^{(Z)}$Phe and Their Tentative Assignments (in %, PED >10% Shown) Based on Calculations[a]

FT-IR[b]	FT-NR[b]	SERS	assignment
3400m			100 ν(NH)
3247m			100 ν(NH)
	3066w		96 $^{Ph}1$
	3051w		94 ν(=CH)
	2995w		92 $\nu_{as}(CH_3)_{Boc}$
	2977w		95 $\nu_{as}(CH_3)_{Boc}$
	2930w		98 $\nu_{s}(CH_3)_{Boc}$
	1709m		74 ν(C=O)$_{COOH}$
1693vs	~1690 vw		73 amide I_2
1672s	~1672 vw		72 amide I_1
1647m,sh	1647vs/ 1650s[c]	1642s	57 $\nu(C_{\alpha 1}{=}C_{\beta})$
	1601s/ 1601s[c]	1596vs	65 ^{Ph}8a
1542s	1542vw		57 amide II_1, 21 amide II_2
1526s			44 amide II_2, 14 amide II_1, 12 $\delta(CH_2)_{Gly}$
1450m	1450w	1446vw	73 $\delta(CH_2)_{Gly}$
1412s	1413w		82 $\delta(CH_3)_{Boc}$
1394m			50 ρ(=CH), 11 νCN_{amide1}
1367m			24 $\omega(CH_2)_{Gly}$, 12 ν(CC), 10 δ(COH)
		1385m	$\nu_s(COO^-)$
1290s	1282w	1290w	60 ^{Ph}3
1245s	1239w		65 $\tau(CH_2)_{Gly}$
	1214m	1209m	34 amideIII$_2$, 18 $\tau(CH_2)_{Gly}$
	1183m	1181m	68 ^{Ph}9a
1170s			35 $\rho(CH_3)_{Boc}$, 26 $\nu(CO)_{Boc}$
1048w	1049vw	1045w	33 $\rho(CH_3)_{Boc}$, 13 $\nu(CO)_{Boc}$
1029w	1032w	1030w,sh	76 ^{Ph}18a
	1002m	998m	79 ^{Ph}12
	925vw	927m	71 ^{Ph}17b, 18 ω(=CH)
	551w	549m	18 $\tau(COO^-)$

[a]B3LYP/6-311++G(d,p). [b]Band positions from the spectra of the solid sample. [c]Raman band positions from the spectra of the solution at pH 11: ν, stretching; δ, scissoring; ρ, rocking; ω, wagging; β, in-plane bending; τ, twisting; s, symmetric; as, asymmetric; vs, very strong; s, strong; m, medium; w, weak; vw, very weak; sh, shoulder. Modes of the phenyl ring (^{Ph}) are given according to the Wilson notation.[37]

disturbs evidently the electron cloud between the neighboring C atoms of the $C_{\alpha 1}{=}C_{\beta}$ bond and the phenyl ring, leading consequently to a change in the polarizabilities. This change is reflected by values of partial atomic charges calculated by the atomic polarized tensor approach (detailed data not shown).[43] The atomic charges of the C_{β} atom are +0.279 and +0.090 au for $\Delta^{(Z)}$Phe and $\Delta^{(E)}$Phe, respectively (the corresponding C atom in Boc-Gly-ΔAla has a charge of −0.136 au). This points out that the phenyl ring in $\Delta^{(E)}$Phe is "isolated" from the $C_{\alpha 1}{=}C_{\beta}$ bond, since the charge of the C_{β} atom is typical for the sole benzene. In turn, the alternation of intensity ratio observed here between the 8a and 12 modes is similar to that found for *trans*- and *cis*-stilbene.[44,45] It has been established that the planarity of the molecule around the central C=C moiety is less disturbed for the *trans* than the *cis* isomer, leading to π-conjugation in the *trans* isomer. Raman spectra of both stilbenes have shown that I_{8a}/I_{12} ratio is ca. 3 and 1 for the *trans* and *cis* molecules, similarly to our *Z* and *E* isomers of ΔPhe. Lowering the I_{8a}/I_{12} ratio in *cis*-stilbene has been explained by reduction of conjugation within the $C_{\alpha 1}{=}C_{\beta}$—Ph that does not result in coupling of vibrations of this moiety. The similar Raman picture is observed for the fully conjugated styrene.[42] In the case of the molecules studied here, the atomic charge differences in the phenyl ring of both isomers are limited to the C_{γ} atom only (see Scheme 1). Namely, this C atomic charge is close to zero in the weakly coupled ring of $\Delta^{(E)}$Phe, as expected, whereas it becomes more negative (−0.114 au) in Boc-Gly-$\Delta^{(Z)}$Phe. This clearly shows an electron perturbation in $\Delta^{(Z)}$Phe due to the resonance with the $C_{\alpha 1}{=}C_{\beta}$ bond affecting the intensity of the their modes.

3.3. Comparison of the Dehydropeptide−Metal Interactions. The SERS experiment collected for solutions of the dehydropeptides at pH 6 does not show an enhancement of Raman scattering, on the contrary to solutions prepared at pH 11 and next mixed with Ag colloid (1:50). No data concerning the acidity of the ionic species of the compounds presented here have been found in the literature, but potentiometric studies of di-, tri-, and tetradehydropeptides containing ΔAla, ΔPhe, and ΔLeu with the free C and N terminal groups have revealed the two protonation constants with values of ~3 and ~9.[8,46,47] It comes out therefore that the majority species in 0.1 and 1×10^{-3} M solutions of the presented Δ-dipeptides at pH 11 will be the anionic species. Normal Raman spectra of 0.1 M solutions at pH 6 and 11 (see Figure 5) are dominated mainly by bands of the solvent (methanol); therefore, only the range 1550−1750 cm^{-1} is presented. However, all the spectra show the disappearance of a band at ca. 1710 cm^{-1} at the higher pH, originating from the ν(C=O) of the terminal acid COOH group. This implies that the anionic form (with COO^-) is present in the solution under the experimental conditions of the recorded SERS spectra and the observed surface enhancement at pH 11 of the adsorbate is related to the presence of the deprotonated carboxylic group.

It has been widely known that colloidal particles of silver usually have a negatively charged surface due to adsorbed reagent anions and hence an adsorbate must exhibit a sufficient affinity to the metal surface to observe the SERS effect.[48,49] However, it has been demonstrated that the oxygen lone electron pair of the deprotonated carboxylic group has a high affinity to the Ag surface. This is verified by the presence of a broad SERS band in the region 1380−1420 cm^{-1} that is attributed to the $\nu_s(COO^-)$ mode. The broadening of this band upon interaction with the metal surface indicates a chemisorptive mode of adsorption.[50−53] The SERS spectra of the dehydropeptides are presented in Figure 6. The normal Raman spectra of the solid samples recorded by using an excitation line at 532 nm are shown in the Supporting Information (Figure 4S). The band intensity ratio in these spectra is the same as that in FT-Raman spectra presented in Figure 3.

The Raman bands of the dipeptides studied here are not observed in normal Raman spectra of the solutions at low concentration used in the SERS experiment ($c = 1 \times 10^{-5}$ M). Then, the spectra shown in Figure 6 are exclusively due to surface enhancement of the Raman scattering of adsorbed molecules by silver nanoparticles. At first glance, the comparison of these spectra with FT-Raman spectra of the solid samples (in Figure 4) indicates the appearance of relatively strong bands at 1362, 1385, and 1387 cm^{-1} in SERS spectra of Boc-Gly-ΔAla, Boc-Gly-$\Delta^{(Z)}$Phe, and Boc-Gly-$\Delta^{(E)}$Phe, respectively. These bands are assigned to the

Table 4. Positions of the Selected IR, Raman, and SERS Bands (in cm^{-1}) of Boc-Gly-$\Delta^{(E)}$Phe and Their Tentative Assignments (in %, PED >10% Shown) Based on Calculations[a]

FT-IR[b]	FT-NR[b]	SERS	assignment
3350vs	3349m		100 ν(NH)
	3057vs		98 $^{Ph}1$
	3024vw		94 ν(=CH)
	2992s		89 $\nu_{as}(CH_3)_{Boc}$
	2981s,sh		93 $\nu_{as}(CH_3)_{Boc}$
	2934vs		91 $\nu_{s}(CH_3)_{Boc}$
1706s,sh	1706m		43 $\nu(C{=}O)_{COOH}$, 30 amide I_2
1692vs	1692w,sh		44 amide I_2, 21 $\nu(C{=}O)_{COOH}$
1647m,sh	1648vs/1640s[c]	1637vs	58 $\nu(C_{\alpha 1}{=}C_{\beta})$
1627m			65 amide I_1
	1599s/1603s[c]	1598vs	70 $^{Ph}8a$
1542s,sh	1544w		62 amide II_1
1527vs	1528w		55 amide II_2
1441m	1448m		71 $\delta(CH_3)_{Boc}$
1414m	1415w		75 $\delta(CH_2)_{Gly}$
1391w			34 ρ(=CH), 13 νCN_{amide1}
		1387s,br	$\nu_{s}(COO^{-})$
		1325m,sh	37 $^{Ph}14$, 24 $\omega(CH_2)_{Gly}$
1286m		1285w	68 $^{Ph}3$
	1265m		36 amideIII_1, 21 $\nu(C_{Ph}{-}C{=}C)$
1249s	1249m,sh		35 amideIII_2, 17 $\nu(CO)_{Boc}$
1214m	1218w	1216m	16 ν(CN), 12 $\tau(CH_2)_{Gly}$
	1185vw	1179m	73 $^{Ph}9a$
1168s			40 $\rho(CH_3)_{Boc}$, 28 $\nu(CO)_{Boc}$
1058m	1060w	1049vw	35 $\rho(CH_3)_{Boc}$, 14 $\nu(CO)_{Boc}$
	1032m	1027vw	65 $^{Ph}18a$
	1001vs	998s	80 $^{Ph}12$
965vw		962w	44 β(CNC), 14 ν(CC)
	923m	927vw	78 $^{Ph}17b$, 17 ω(=CH)
	772m		38 ν(CC), 20 $\beta(CO)_{Boc}$
692m			90 $^{Ph}5$

[a]B3LYP/6-311++G(d,p). [b]Band positions from the spectra of the solid sample. [c]Raman band positions from the spectra of the solution at pH 11: ν, stretching; δ, scissoring; ρ, rocking; ω, wagging; β, in-plane bending; τ, twisting; s, symmetric; as, asymmetric; vs, very strong; s, strong; m, medium; w, weak; vw, very weak; sh, shoulder. Modes of the phenyl ring (^{Ph}) are given according to the Wilson notation.[37]

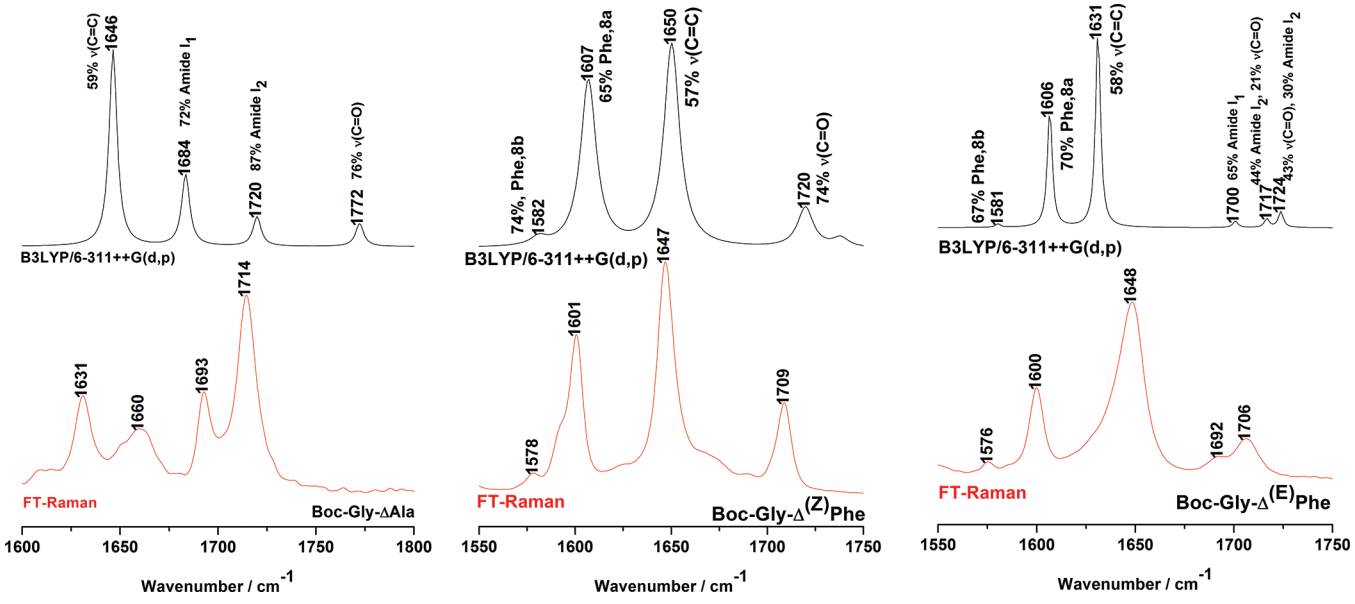

Figure 4. Comparison of the FT-Raman experimental (solids) and theoretical spectra in the region 1550−1750 cm^{-1} with the assignment of the bands (% denotes contribution of a vibration in PED).

dx.doi.org/10.1021/jp208586j | J. Phys. Chem. B 2012, 116, 1414−1425

Scheme 2. Possible Resonance Structures of the Dehydroamide Moiety[10]

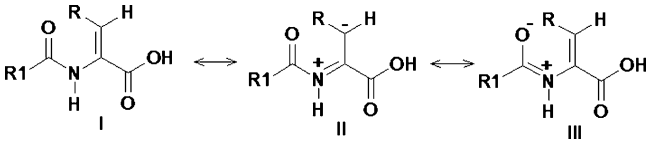

$\nu_s(COO^-)$ mode, as we briefly discussed above. Hence, the adsorption on the silver nanoparticles essentially involves the ionized carboxylic groups. The comparison of relative intensities within each SERS spectrum in Figure 6 shows that the $\nu_s(COO^-)$ mode is more enhanced in the case of the ΔAla and $\Delta^{(E)}$Phe dehydropeptides than for the $\Delta^{(Z)}$Phe one. The other pronounced features of the presented SERS spectra are the strongly enhanced bands of the benzylidene moiety in the region 1600−1660 cm^{-1} that are discussed below.

The analysis of the SERS spectrum of the ΔAla dehydropeptide points out that the ionized carboxylic group interacts directly with the silver surface (Figure 6, Table 2). The normal Raman spectrum of the alkaline solution of this dehydropeptide shows a weak band at 1393 cm^{-1} (data not shown) that could be attributed to the $\nu_s(COO^-)$ vibration; however, this region of the spectrum shows mainly strong bands of methanol, making this assignment uncertain. Keeping in mind that the relatively sharp SERS band is observed at 1362 cm^{-1}, this could suggest the red shift of this mode by 30 cm^{-1}. Such a significant shift indicates strong chemical interaction of the COO^- group with Ag, thus suggesting the possibility of significant contribution of a charge-transfer mechanism to SERS enhancement of this band. Also, the SERS enhancement of a band at 610 cm^{-1} that originates mainly from the coupling of the $\beta(COO^-)$ (31% PED) and $\rho(C{=}O)_{amide1}$ (25% PED) modes occurs in the SERS spectrum of Boc-Gly-ΔAla. One would expect strong and red-shifted by more than 10 cm^{-1} $\nu_s(COO^-)$ and very weak $\beta(COO^-)$ bands in SERS when the carboxylate group adsorbs on the metal surface via π orbital in a flat orientation.[53−55] Since in the SERS spectrum (Figure 6) both discussed bands are of comparative intensity, it seems that the tilted orientation is more likely. Moreover, the significant broadening of the $\nu_s(COO)$ band generally indicates various

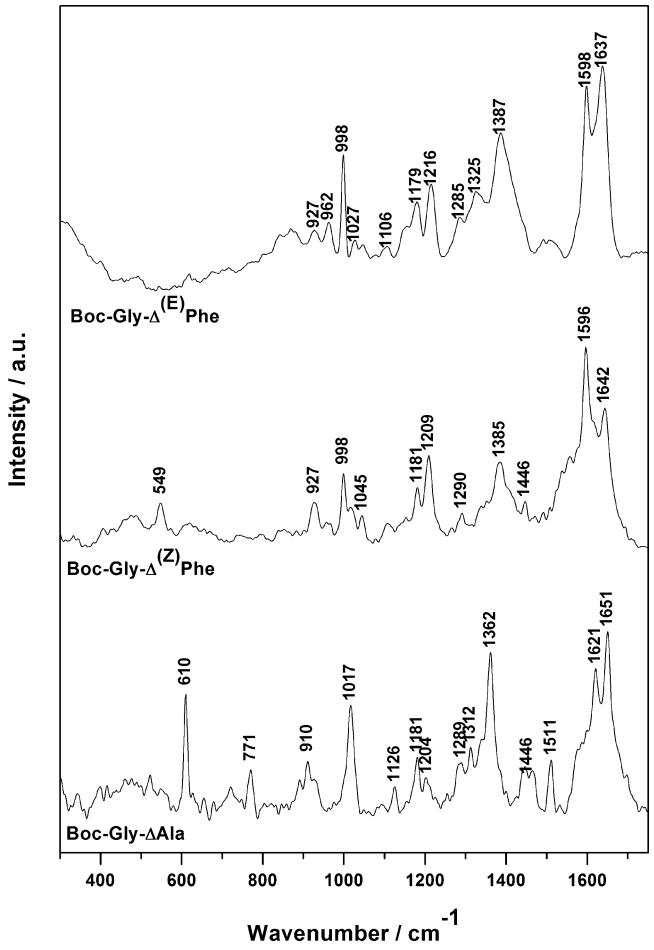

Figure 6. SERS spectra of the dehydropeptides studied (at pH 11) in the region 300−1800 cm^{-1} (an excitation line at 532 nm).

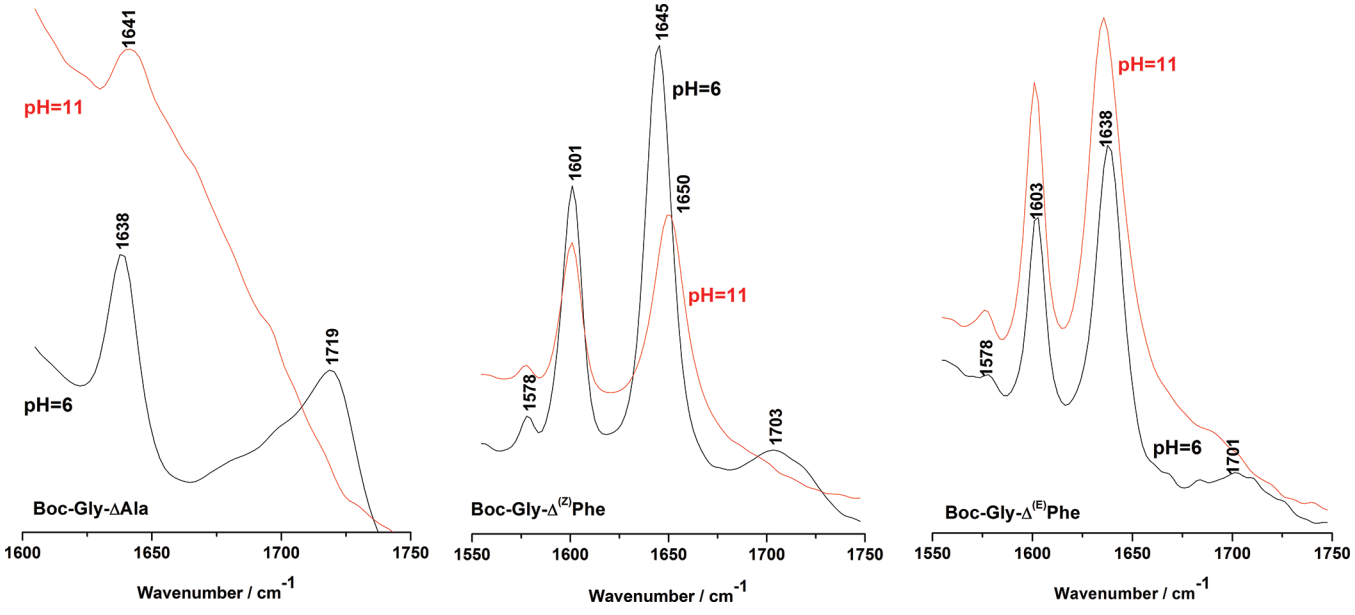

Figure 5. FT-Raman spectra in the region 1550−1750 cm^{-1} of the dehydropeptides solutions (0.1 M) at pH 6 and 11.

dx.doi.org/10.1021/jp208586j | J. Phys. Chem. B 2012, 116, 1414−1425

orientations of an analyte on the metal surface,[50−52] while here it is relatively narrow in comparison to SERS of the other dehydropeptides (cf. Figure 6). This results rather from a uniform pattern of Ag coordination by the carboxylate group of the ΔAla derivative. Furthermore, the close proximity of the peptide group changes the spatial arrangement of the backbone. Thus, the conjugated fragment O═C—(N)H—C═CH_2 leads to the appearance of the surface enhancement of vibrations originating from this molecular fragment, i.e., $\nu(C_{\alpha 1}{=}C_{\beta})$ at 1621 cm^{-1} and amide I/amide II at 1651 and 1511 cm^{-1}, respectively. According to the PED assignment (see Table 2), the amide I mode at 1651 cm^{-1} comes from vibration of the amide 1 bond (cf. Scheme 1), whereas both amide groups of the molecule contribute to the amide II mode at 1511 cm^{-1}. One notes that the relative intensity of the $\nu(C_{\alpha 1}{=}C_{\beta})$/amide I bands decreases due to adsorption on the metal surface (compare Figures 4 and 6). This indicates that upon adsorption the change of polarizability of the amide I vibration is more perpendicular to the surface than this in the >C═CH_2 group. In turn, the SERS intensity of the amide I mode at 1651 cm^{-1} is similar to the intensity of the $\nu_s(COO^-)$ band at 1362 cm^{-1}. If the mode with the main contribution of the ν(C═O) vibration is enhanced so strongly, this may imply interaction of the amide C═O group with the metal particles in a vertical orientation with respect to the metal surface. There are several SERS bands due to the methyl groups in the Boc moiety. The strong band at 1017 cm^{-1} is due to the CH_3 rocking vibration, while the scissoring mode of the methyl groups and the in-plane bending vibrations of the C—C and C—O bonds of the Boc group are observed at 1446 and 771 cm^{-1}, respectively. We interpret the relative strength of these bands as evidence that the modes of the Boc group have components of Raman polarizability perpendicular to the metal surface. The similar enhancement of the bands assigned to vibrations of methyl groups has been found for SERS of alanine.[56] On the basis of the aforementioned elucidations for the enhanced bands and SERS mechanism, we propose the schematic adsorption mode of Boc-Gly-ΔAla in Figure 7A. As seen from Table 2, most SERS bands are red-shifted by at least 10 cm^{-1} in comparison to corresponding bands in the normal Raman spectra (Figure 3 and Figure 3S in the Supporting Information). Such a shifting suggests strong chemical interaction with the surface (chemisorption). Thus, we can conclude that a charge-transfer mechanism may contribute to the surface enhancement of the Raman spectrum of Boc-Gly-ΔAla, besides the dominating electromagnetic enhancement.

As seen from the SERS spectra of the peptides containing ΔPhe (Figure 6, Tables 3 and 4), the symmetric stretching mode of the COO^- group appears at the same position (ca. 1385 cm^{-1}) but with totally different relative intensities. The stronger enhancement of this band for the $\Delta^{(E)}$Phe derivative suggests a more perpendicular orientation of this group on the Ag surface than for the *Z* isomer. An interesting conclusion can be drawn regarding the SERS bands arising from the Ph and $\nu(C_{\alpha 1}{=}C_{\beta})$ modes. The most characteristic bands of the phenyl ring, 8a and 12, appear in the SERS spectra almost in the same position as their corresponding NR counterparts, i.e., near 1600 and 998 cm^{-1}, respectively (cf. Figures 4 and 6). Moreover, both bands are not remarkably broadened in the SERS spectra (especially 998 cm^{-1}). The fwhm of the 998 and 1600 cm^{-1} bands increases by ca. 2−3 and 4 cm^{-1}, respectively, due to adsorption on the Ag colloid. This observation suggests that there is no direct interaction between the phenyl ring and silver.

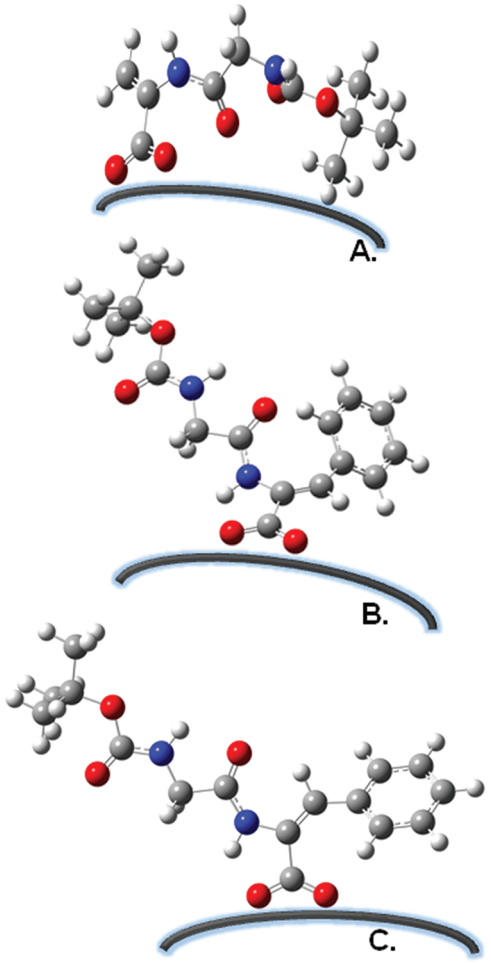

Figure 7. Proposed orientation of Boc-Gly-ΔAla (A), Boc-Gly-$\Delta^{(Z)}$Phe (B), and Boc-Gly-$\Delta^{(E)}$Phe (C) adsorbed on the silver colloidal nanoparticles.

The 1600 cm^{-1} bands are significantly enhanced upon adsorption on the Ag colloid in comparison to the bands in the normal Raman spectrum of the solid. The strong enhancement of the 8a mode in SERS for both molecules can result from some contribution of a charge-transfer effect, as it has been reported in the literature.[50,51] The other slightly enhanced bands of the Ph ring are assigned to the in-plane 14 (1325 cm^{-1}), 3 (ca. 1290 cm^{-1}), and 9a (ca. 1180 cm^{-1}) and out-of-plane 17b (927 cm^{-1}) modes in SERS of both isomers (see Tables 3 and 4). This can suggest that the aromatic moiety adopts a rather slightly tilted orientation on the silver surface.[55,56]

On the other hand, the stretching mode of the $C_{\alpha}{=}C_{\beta}$ bond is red-shifted by 6 and 11 cm^{-1} due to adsorption on the silver particles, for $\Delta^{(Z)}$Phe and $\Delta^{(E)}$Phe, respectively, with respect to their NR counterpart centered at 1648 cm^{-1} in the spectra of the solids (see Tables 3 and 4). In solution, this band is observed at 1651 and 1636 cm^{-1}, respectively. This confirms that the SERS shifting of $\nu(C_{\alpha}{=}C_{\beta})$ is not significant. One can also notice alternation of the relative intensities of 8a (near 1600 cm^{-1}) and $\nu(C_{\alpha}{=}C_{\beta})$ (around 1640 cm^{-1}) (cf. Figure 6); i.e., $I_{\nu(C\alpha{=}C\beta)}/I_{8a}$ is 0.7 and 1.1 for $\Delta^{(Z)}$Phe and $\Delta^{(E)}$Phe, respectively. A ratio of 1.6 was found for the conjugated $C_{\alpha}{=}C_{\beta}$—Ph moiety in $\Delta^{(Z)}$Phe in the solution and solid state. Hence, some conjugation of both modes should be considered

dx.doi.org/10.1021/jp208586j | J. Phys. Chem. B 2012, 116, 1414−1425

as a result of a flow of the electron density from the π electron cloud localized in the benzylidene fragment due to the adsorbate−metal interaction. Keeping in mind spatial localization of the ΔPhe residues in the peptide backbone (see Figure 1B,C) and adsorption through the COO^- group, closer proximity of the —C═C—Ph to the metal spheres should be expected in $\Delta^{(E)}$Phe. Thus, a more perpendicular change of polarizability of $\nu(C_\alpha{=}C_\beta)$ may be expected for the *E* isomer. The medium-intensity SERS bands at 1209 and 1216 cm^{-1} appear for the $\Delta^{(Z)}$Phe and $\Delta^{(E)}$Phe derivatives, respectively. They are ascribed to out-of-plane vibrations involving Gly and the second amide bond for both molecules. Moreover, absence or weak involvement of the Boc methyl groups in the surface adsorption is rather expected, because no SERS active bands observed here originate from vibrations of the Boc group (see Tables 3 and 4). Schematic pictures of the possible adsorption geometry of Boc-Gly-$\Delta^{(Z)}$Phe and Boc-Gly-$\Delta^{(E)}$Phe are shown in Figure 7B and C, respectively. It is worth mentioning that, on the contrary to SERS of Boc-Gly-ΔAla, the SERS spectra of both *Z* and *E* isomers of Boc-Gly-ΔPhe exhibit the absence of the amide I bands. These bands can be overlapped by the other strong bands in the region 1550−1700 cm^{-1}, or simply the orientation of the amide group with respect to the surface may result in a very small value of the component of polarizability change of the amide vibration, perpendicular to the surface. Moreover, the larger distance of the CO amide groups from the surface in the case of adsorbed Boc-Gly-$\Delta^{(Z)}$Phe and Boc-Gly-$\Delta^{(E)}$Phe, as compared with Boc-Gly-ΔAla (see Figure 7), may also result in considerable weakening of the electromagnetic enhancement of the amide I bands for those two compounds. Furthermore, the wavenumbers and widths of all SERS bands of both isomers are not affected significantly by the interaction with the metal particles. Thus, one can deduce that in this case the contribution of the chemical enhancement to SERS is rather small and surface enhancement of the spectrum is strongly determined by electromagnetic mechanism.

4. CONCLUSIONS

In this report, we attempted to relate the full vibrational information obtained for the solid samples of three peptides to the structure and chemical nature of the dehydroresidues (ΔAla and ΔPhe). The detailed analysis of vibrations of the amide and unsaturated residue was assisted with DFT calculations. This permitted the correlation between the molecular structure and spectral profile of each molecule. Our results supported the tendency of dehydroalanine to constrain the extended conformation of the peptide chain, whereas the presence of dehydrophenylalanine inclines a turn of the peptide backbone. Interesting conclusions can be drawn from Raman spectra shown here for the first time for dehydropeptides. Due to the presence of the C═C bond, the dehydroresidues are good Raman scatters and their Raman bands can provide explicit information on interatomic interactions within the peptide molecule. In turn, SERS spectroscopy revealed the all studied peptides need to be deprotonated to adsorb effectively on the Ag nanoparticles and thereby yield considerably enhanced Raman signal. Interaction with the metal surface through the carboxylate group is different for all molecules and is reflected in the various positions and line widths of a band at ca. 1360−1390 cm^{-1}. The size and conformation of the dehydroresidue affects the adsorption geometry significantly. In each case, the presence of the unsaturated fragment in close proximity to the Ag particles is evidenced by strong enhancement of its characteristic vibrations.

■ ASSOCIATED CONTENT

Supporting Information

(i) Comparison of experimental and computed spectra of Boc-Gly-ΔAla (Figure 1S). (ii) Comparison of experimental and computed spectra of Boc-Gly-$\Delta^{(Z)}$Phe (Figure 2S). (iii) Comparison of experimental and computed spectra of Boc-Gly-$\Delta^{(E)}$Phe (Figure 3S). (iv) Normal Raman spectra of the solid peptides studied recorded by using the 532 nm excitation line in the spectral range 200−1800 cm^{-1} (Figure 4S). (v) Definitions of the internal coordinates used in Tables 2−4. This material is available free of charge via the Internet at http://pubs.acs.org.

■ AUTHOR INFORMATION

Corresponding Author

*E-mail: malek@chemia.uj.edu.pl. Phone: +48 12 663 2064. Fax: +48 12 634 0515.

■ ACKNOWLEDGMENTS

K.M. would like to thank the Polish Ministry of Science and Higher Education for the financial support (Grant No. N N204 333037 in 2009−2011). Calculations were done at the Academic Computer Center "Cyfronet", Krakow, Poland (Grant MNiI/SGI2800/UJ/003/2005), which is acknowledged for computing time.

■ REFERENCES

(1) Rink, R.; Wierenga, J.; Kuipers, A.; Kluskens, L. D.; Driessen, A. J. M.; Kuipers, O. P. *Appl. Environ. Microbiol.* **2007**, *73*, 1792−1796.
(2) Bagley, M. C.; Dale, J. W.; Merritt, E. A.; Xiong, X. *Chem. Rev.* **2005**, *105*, 685−714.
(3) Brotz, H.; Sahl, H. G. *J. Antimicrob. Chemother.* **2000**, *46*, 1−6.
(4) Grigoryan, H. A.; Hambardzumyana, A. A.; Mkrtchyan, M. V.; Topuzyan, V. O.; Halebyan, G. P.; Asatryan, R. S. *Chem.-Biol. Interact.* **2008**, *171*, 108−116.
(5) Latajka, R.; Lewginski, M.; Makowski, M.; Pawelczak, M.; Huber, T.; Sewald, N.; Kafarski, P. *J. Pept. Sci.* **2008**, *14*, 1084−1094.
(6) Langer, M.; Pauling, A.; Retey, J. *Angew. Chem., Int. Ed. Engl.* **1995**, *34*, 1464−1465.
(7) Gupta, A.; Chauhan, V. S. *Biopolymers* **1990**, *30*, 395−403.
(8) Brasun, J.; Makowski, M.; Oldziej, S.; Swiatek-Kozlowska, J. *J. Inorg. Biochem.* **2004**, *98*, 1391−1398.
(9) Sigh, T. P.; Kaur, P. *Prog. Biophys. Mol. Biol.* **1996**, *66*, 141−165.
(10) Broda, M. A.; Siodlak, D.; Rzeszotarska, B. *J. Pept. Sci.* **2005**, *11*, 546−555.
(11) Gupta, A.; Mehrotra, R.; Klimov, E.; Siesler, H. W.; Joshi, R. M.; Chauhan, V. S. *Chem. Biodiversity* **2006**, *3*, 284−295.
(12) Makowski, M.; Brzuszkiewicz, A.; Lisowski, M.; Lis, T. *Acta Crystallogr., Sect. C: Cryst. Struct. Commun.* **2005**, *61*, o424−o426.
(13) Makowski, M.; Lisowski, M.; Maciag, A.; Lis, T. *Acta Crystallogr., Sect. E: Struct. Rep. Online* **2006**, *62*, o807−o810.
(14) Makowski, M.; Lisowski, M.; Mikolajczyk, I.; Lis, T. *Acta Crystallogr., Sect. E: Struct. Rep. Online* **2007**, *63*, o19−o21.
(15) Jain, R. M.; Rajashankar, K. R.; Ramakumar, S.; Chauhan, V. S. *J. Am. Chem. Soc.* **1997**, *119*, 3205−3211.
(16) Aleman, C. *Biopolymers* **1994**, *34*, 841−847.
(17) Inai, Y.; Sakakura, Y.; Hirabayashi, T. *Polym. J.* **1998**, *30*, 828−832.
(18) Gupta, A.; Mehrotra, R.; Tewari, J.; Jain, R. M.; Chauhan, V. S. *Biopolymers* **1999**, *50*, 595−601.
(19) Broda, M. A.; Rzeszotarska, B.; Smelka, L.; Rospenk, M. *J. Pept. Res.* **1997**, *50*, 342−351.

(20) Stevenson, R.; Stokes, R. J.; MacMillan, D.; Armstrong, D.; Faulds, K.; Wadsworth, R.; Kunuthur, S.; Suckling, C. J.; Graham, D. *Analyst* **2009**, *134*, 1561−1564.
(21) Pan, Z.; Morgan, S. H.; Ueda, A.; Mu, R.; Cui, Y.; Guo, M.; Burger, A.; Yeh, Y. *J. Raman Spectrosc.* **2005**, *36*, 1082−1087.
(22) Kneipp, J.; Kneipp, H.; Wittig, B.; Kneipp, K. *Nanomedicine* **2010**, *6*, 214−226.
(23) Qian, X.-M.; Nie, S. M. *Chem. Soc. Rev.* **2008**, *37*, 912−920.
(24) Hering, K.; Cialla, D.; Ackermann, K.; Dorfer, T.; Moller, R.; Schneidewind, H.; Mattheis, R.; Fritzsche, W.; Rosch, P.; Popp, J. *Anal. Bioanal. Chem.* **2008**, *390*, 113−124.
(25) Makowski, M.; Rzeszotarska, B.; Kubica, Z.; Wieczorek, P. *Liebigs Ann. Chem.* **1984**, *No. 5*, 920−928.
(26) Makowski, M.; Rzeszotarska, B.; Pietrzynski, G.; Kubica, Z. *Liebigs Ann. Chem.* **1985**, *No. 5*, 893−900.
(27) Makowski, M.; Rzeszotarska, B.; Smelka, L.; Kubica, Z. *Liebigs Ann. Chem.* **1985**, *No. 7*, 1457−1464.
(28) Creighton, J. A.; Blatchford, C. G.; Albrecht, M. G. *J. Chem. Soc.* **1979**, *75*, 790−798.
(29) Chowdhury, J.; Ghosh, M.; Misra, T. N. *J. Colloid Interface Sci.* **2000**, *228*, 372−378.
(30) Yaffe, N. R.; Blanch, E. W. *Vib. Spectrosc.* **2008**, *48*, 196−201.
(31) Frisch, M. J.; Trucks, G. W.; Schlegel, H. B.; Scuseria, G. E.; Robb, M. A.; Cheeseman, J. R.; Montgomery, J. A., Jr.; Vreven, T.; Kudin, K. N.; Burant, J. C.; et al. *Gaussian 09*, revision A. 1; Gaussian, Inc.: Wallingford, CT, 2009.
(32) Lee, C.; Yang, W.; Parr., R. G. *Phys. Rev. B: Condens. Matter Mater. Phys.* **1988**, *37*, 785−789.
(33) Becke, A. D. *J. Chem. Phys.* **1993**, *98*, 5648−5652.
(34) Michalska, D.; Wysokinski, R. *Chem. Phys. Lett.* **2005**, *403*, 211−217.
(35) Fogarasi, G.; Zhou, X.; Taylor, P. W.; Pulay, P. *J. Am. Chem. Soc.* **1992**, *114*, 8191−8201.
(36) Pulay, P.; Fogarasi, G.; Pang, F.; Boggs, J. E. *J. Am. Chem. Soc.* **1979**, *101*, 2550−2560.
(37) Martin, J. M. L.; Van Alsenoy, C. *Gar2ped*; University of Antwerp, 1995.
(38) Zanuy, D.; Rodriguez-Ropero, F.; Nussinov, R.; Aleman, C. *J. Struct. Biol.* **2007**, *160*, 177−189.
(39) Makowski, M.; Lisowski, M.; Mikolajczyk, I.; Lis, T. *Acta Crystallogr., Sect. E: Struct. Rep. Online* **2007**, *E63*, o989−o991.
(40) Broda, M. A.; Buczek, A.; Siodlak, D.; Rzeszotarska, B. *J. Pept. Sci.* **2009**, *15*, 465−473.
(41) Broda, M. A.; Rospenk, M.; Siodlak, D.; Rzeszotarska, B. *J. Mol. Struct.* **2005**, *740*, 17−24.
(42) Varsanyi, G. *Assignments for vibrational spectra of 700 benzene derivatives*; Akademiai Kiado: Budapest, Hungary, 1973; pp 46−87.
(43) Cioslowski, J. *J. Am. Chem. Soc.* **1989**, *111*, 8333−8336.
(44) Kumar, K.; Phelps, D. J.; Carey, P. R. *Can. J. Chem.* **1978**, *56*, 232−239.
(45) Furuya, K.; Kawato, K.; Yokoyama, H.; Sakamoto, A.; Tasumi, M. *J. Phys. Chem. A* **2003**, *107*, 8251−8256.
(46) Jezowska-Bojczuk, M.; Varnagy, K.; Sovago, I.; Pietrzynski, G.; Dyba, M.; Kubica, Z.; Rzeszotarska, B.; Smelka, L.; Kozlowski, H. *J. Chem. Soc., Dalton Trans.* **1996**, *No. 15*, 3265−3268.
(47) Swiatek-Kozlowska, J.; Brasun, J.; Chruscinski, L.; Chruscinka, E.; Makowski, M.; Kozlowski, H. *New J. Chem.* **2000**, *24*, 893−896.
(48) Bell, S. E. J.; Sirimuthu, N. M. S. *J. Phys. Chem. B* **2005**, *109*, 3787−3792.
(49) Sekine, R.; Vongsvivut, J.; Robertson, E. G.; Spiccia, L.; McNaughton, D. *J. Phys. Chem. B* **2010**, *114*, 7104−7111.
(50) Castro, J. L.; Lopez-Raminez, M. R.; Lopez Tocon, I.; Otero, J. C. *J. Colloid Interface Sci.* **2003**, *263*, 357−363.
(51) Lopez-Ramirez, M. R.; Garcia-Ramos, J. V.; Otero, J. C.; Castro, J. L.; Sanchez-Cortes, S. *Chem. Phys. Lett.* **2007**, *446*, 380−384.
(52) Seballos, L.; Richards, N.; Stevens, D. J.; Patel, M.; Kapitzky, L.; Lokey, S.; Millhauser, G.; Zhang, J. Z. *Chem. Phys. Lett.* **2007**, *447*, 335−339.
(53) Fleger, Y.; Mastai, Y.; Rosenbluh, M.; Dressler, D. H. *J. Raman Spectrosc.* **2009**, *40*, 1572−1577.
(54) Kwon, Y. J.; Son, D. H.; Ahn, S. J.; Kim, M. S.; Kim, K. *J. Phys. Chem.* **1994**, *98*, 8481−8487.
(55) Suh, J. S.; Kim, J. *J. Raman Spectrosc.* **1998**, *29*, 143−148.
(56) Suh, J. S.; Moskovits, M. *J. Am. Chem. Soc.* **1986**, *108*, 4711−4718.